PRAMANA
— journal of
physics

© Indian Academy of Sciences

Vol. 58, Nos 5 & 6
May & June 2002
pp. 893–898

Investigating the vortex melting phenomenon in BSCCO crystals using magneto-optical imaging technique

A SOIBEL[1,*], S S BANERJEE[1], Y MYASOEDOV[1], M L RAPPAPORT[1], E ZELDOV[1], S OOI[2] and T TAMEGAI[2,3]

[1]Department of Condensed Matter Physics, The Weizmann Institute of Science, Rehovot 76100, Israel

[2]Department of Applied Physics, The University of Tokyo, Hongo, Bunkyo-ku, Tokyo 113-8656, Japan

[3]CREST, Japan Science and Technology Corporation (JST), Japan

*Email: Eli.zeldov@weizmann.ac.il

Abstract. Using a novel differential magneto-optical imaging technique we investigate the phenomenon of vortex lattice melting in crystals of $Bi_2Sr_2CaCu_2O_8$ (BSCCO). The images of melting reveal complex patterns in the formation and evolution of the vortex solid–liquid interface with varying field (H)/temperature (T). We believe that the complex melting patterns are due to a random distribution of material disorder/inhomogeneities across the sample, which create fluctuations in the local melting temperature or field value. To study the fluctuations in the local melting temperature/field, we have constructed maps of the melting landscape $T_m(H, r)$, viz., the melting temperature (T_m) at a given location (r) in the sample at a given field (H). A study of these melting landscapes reveals an unexpected feature: the melting landscape is not fixed, but changes rather dramatically with varying field and temperature along the melting line. It is concluded that the changes in both the scale and shape of the landscape result from the competing contributions of different types of quenched disorder which have opposite effects on the local melting transition.

Keywords. Vortices; melting; BSCCO; magneto-optical imaging.

PACS Nos 74.60.Ec; 74.60.Ge; 74.60.Jg; 74.72.Hs

1. Introduction

General arguments [1] suggest that weak disorder results in a rounding of the first-order transition while extensive disorder transforms it into second order, yet the details of this ubiquitous process on the atomic level are still not clear. The vortex lattice in superconductors provides a unique and a relatively easy way to study this first-order transition [2,3] over a wide range of particle densities, by just varying the magnetic field at different temperatures. By the use of a novel differential magneto-optical imaging technique, a direct experimental visualization of the melting process in a disordered system is obtained, revealing complex melting patterns. From the images of melting at different fields and temperatures we investigate the behavior of the local melting temperature at different fields,

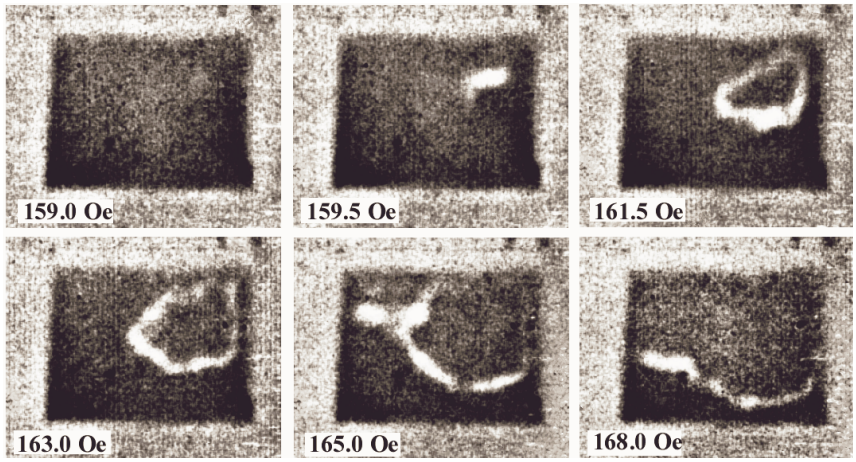

Figure 1. Vortex lattice melting process in a small BSCCO crystal. Differential MO images of the melting process in a BSCCO crystal ($T_c = 90$ K) of area 0.35×0.27 mm^2 at $T = 60$ K and $H_a \parallel c$-axis. The gray scale from black to white spans a field range of 0.2 G. The region outside the sample is bright. The differential images are obtained by subtracting the image at field H_a from the image at $H_a + \delta H_a$, with $\delta H_a = 1$ Oe. A detailed discussion of the images can be found in the text.

viz., we construct the melting landscape $T_m(H,\ r)$. Such a map has revealed a competition between different types of pinning arising out of sample inhomogeneities/disorder. Different types of pinning have opposite effect on the local value of melting T/H.

2. The differential magneto-optical technique

Briefly, the MO imaging is achieved by placing a garnet indicator film on a sample. Linearly polarized light undergoes Faraday rotation in the indicator and reflected back through a crossed polarizer, resulting in a real-time image of the magnetic field distribution.

Under equilibrium magnetization conditions, in platelet-shaped samples in perpendicular applied field $H_a \parallel z$, the dome-shaped profile of the internal field [4], which has a maximum in the center, results in the central part of the sample reaching the melting field $H_m(T)$ first upon increasing field or temperature. We should therefore expect the nucleation of a small round 'puddle' of vortex liquid in the center of the sample, surrounded by vortex solid. Due to the first-order nature of the transition, the vortex-lattice melting is associated with a discontinuous step in the equilibrium magnetization [3], $4\pi\,\Delta M = \Delta(B - H)$. Since in our geometry the field H is continuous across the solid–liquid interface, the induction B in the liquid is thus enhanced by ΔB relative to the solid. In BSCCO crystals ΔB is typically 0.1 to 0.4 G [3]. Conventional magneto-optical (MO) imaging techniques [5–7] (see figure 1 caption) cannot resolve such small field differences. We have therefore devised the following differential method.

A MO image is acquired by averaging typically ten consecutive CCD images at fixed H_a and T. Then H_a is increased by $\delta H_a \ll H_a$, or T is increased by $\delta T \ll T$, and a

second averaged image is obtained. The difference between the two images is stored as the differential image. This process is repeated and averaged typically 100 times, yielding field resolution of about 30 mG, which is typically two orders of magnitude better than the standard MO method. By recording the differential images in a sequence of fields or temperatures a 'movie' of the melting process is obtained [8].

In the absence of disorder, as the field is increased by δH_a, the radius of the vortex-liquid puddle in the center of the sample should increase by δR, determined by the gradient of the dome-shaped profile $H(x, y)$. The differential image in this case should show a bright ring on a dark background, which indicates the location of the expanding solid–liquid interface. In the rest of the image almost no change in the field should occur, except the uniform background signal of δH_a. The intensity of the ring is ΔB above the background [9], independent of δH_a, whereas the width of the ring reflects the distance δR over which the interface expands due to field modulation δH_a.

3. Observation of melting patterns in BSCCO crystals

Figure 1 presents several differential MO images of the vortex-lattice melting at $T = 60$ K in one of the BSCCO crystals, which is initially in the vortex-solid phase. At 159.5 Oe a small liquid puddle is nucleated, seen as a bright spot in the upper-right part. Note that in contrast to the expectations, the puddle is not in the center of the sample, nor is it round, but instead a rather rough shape of the vortex-liquid domain is observed. As the field is further increased, a ring-like bright object is obtained, which is the solid–liquid interface separating the liquid from the surrounding vortex solid. Both the shape and the width of the ring are highly nonuniform. At 165 Oe a 'tongue' of the liquid protrudes sharply to the left side. By 168 Oe the upper part of the sample is entirely in the liquid phase, with a rough interface separating the liquid from the narrow solid region at the bottom. We shall attempt to understand the influence of material disorder/inhomogeneities across the sample on local melting properties.

4. Investigating the melting landscape in BSCCO

Since the differential MO technique enables us to spatially resolve the location of the vortex solid–liquid interface, we attempt to deduce from the melting images the spatial (r) variations in the melting temperature (T_m) at different fields (H) and at different locations (r) in the sample, i.e., $T_m(H, r)$. There have been numerous studies in the past relating to the effect of disorder on the melting phenomenon. Weak point disorder is expected to shift the melting transition to lower temperature, while preserving the first order nature [10,11], while correlated disorder shifts the melting transition to higher temperatures [12,13]. Oxygen doping is another parameter that, apart from affecting the T_c of the sample, changes the material anisotropy, which in turn significantly changes the slope of the melting line [14]. All these different parameters not only determine the location of the mean field melting transition line $T_m(H)$, but should also lead to significant fluctuations in the value of $T_m(H, r)$.

In figures 2a and 2b we present a spatial distribution of the liquid regions nucleating in the sample for different T at a fixed H_a, the various colors indicating areas which melt

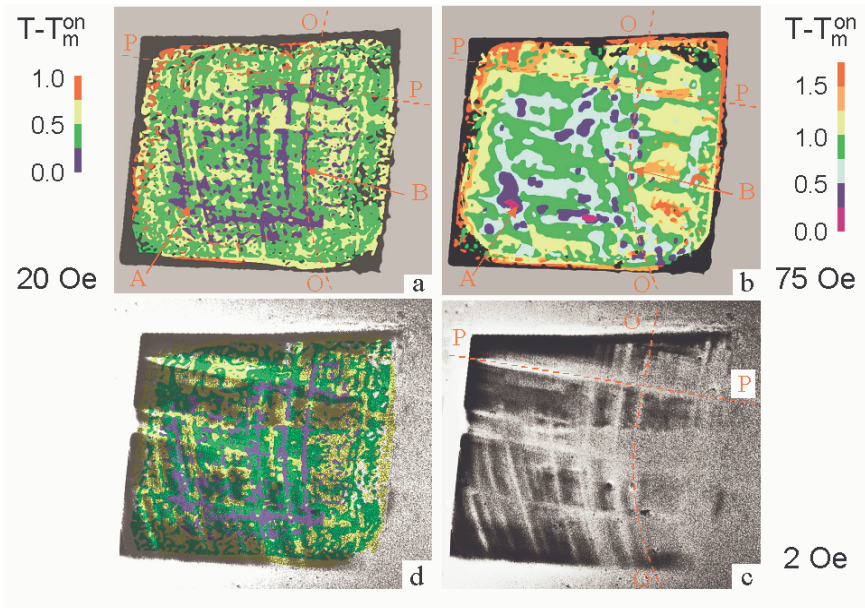

Figure 2. The contours of the melting propagation in BSCCO crystal ($T_c = 91$ K, dimensions $1 \times 1 \times 0.05$ mm^3) at $H_a = 20$ Oe (**a**) and 75 Oe (**b**). The color code indicates the expansion of the liquid domains as the temperature is increased in 0.25 K steps. The onset of melting at $T_m^{on} = 86.25$ K in (**a**) and at 74.25 K in (**b**). (**c**) Differential magneto-optical image of the magnetic field penetration at $H_a = 2$ Oe, $T = 89$ K, $\delta H_a = 1$ Oe. (**d**) Superposition of (**a**) and (**c**).

during a 0.25 K increment in T. Material disorder modifies the local melting temperature, thus forming a complicated $T_m(H, r)$ landscape. Figures 2a and 2b can thus be viewed as 'topographical maps' of the melting landscape at H_a of 20 and 75 Oe, respectively. The minima points or the valleys of the landscape (blue) melt first whereas the peaks of the landscape (red) melt last. The two landscapes in figure 2 are substantially different. In addition to the significant change in the characteristic length scale and roughness of the landscape, there are many regions in the sample that show qualitatively different properties. By comparing the figures for 20 Oe and 75 Oe, one can clearly see how peaks of the melting landscape change into valleys. For example, at 20 Oe the valley in the form of an arc along the 'O–O' dashed line has three long and narrow blue segments, while at 75 Oe, the blue minima have the form of rather circular spots. Also at 75 Oe, to the right of the 'O–O' valley, a number of extended peaks colored yellow and orange can be seen, while at the same locations at 20 Oe we find blue and green valleys. Also, importantly, the width of the transition or the valley-to-peak height, changes significantly. At 20 Oe the entire sample melts within about 1 K, whereas at 75 Oe the melting process spans almost twice this range. We have performed a more quantitative analysis by investigating the melting behavior at several points, eg., at points A and B in figure 2 [15]. We have found that above 85 K the point B systematically melts about 0.5 K below point A and below 85 K, the point B melts up to 2 K above point A. Numerous other points also show similar crossing behavior in

their local melting temperatures. This implies that the valleys in the melting landscape at low fields may turn into peaks at higher fields.

We try to understand the crossing of melting landscape using the generic expression of the melting transition [16], $H_m(T,\ \mathbf{r}) = H_0(\mathbf{r})(1 - T/T_c(\mathbf{r}))^{\alpha(\mathbf{r})}$. We now set $\alpha(\mathbf{r}) = \alpha$ for simplicity and we introduce spatial variations in T_c and H_0 with $T_c(\mathbf{r}) = T_c + \Delta T_c(\mathbf{r})$ and $H_0(\mathbf{r}) = H_0 + \Delta H_0(\mathbf{r})$, we rewrite $H_m(T, \mathbf{r}) = H_m(T) + \Delta H_m(T, \mathbf{r})$. Using these we get the expression $\Delta H_m(T, \mathbf{r}) \simeq [\Delta H_0(\mathbf{r}) + \alpha H_0 \Delta T_c(\mathbf{r})/(T_c - T)](1 - T/T_c)^{\alpha}$ describing the disorder-induced melting landscape. Out of the two terms in the expression, we see that $\Delta H_0(r)$ dominates at low T, while the second term containing $\Delta T_c(r)$ dominates close to T_c. It is the competition arising out of the two terms which causes the crossing over in the melting landscape. To illustrate our point further consider the following: at high temperatures ΔT_c variations should modify the local critical field $H_{c1}(\mathbf{r})$. Figure 2c shows a high-sensitivity image of the initial field penetration into the sample at $H_a = 2$ Oe and $T = 89$ K. A strong correlation between the field penetration form and the melting patterns in figure 2a is readily visible. For a more accurate comparison figure 2d presents a superposition of the penetration image with the melting patterns at 20 Oe. The color in the image is given by the melting contours, while the brightness is defined by the penetration field. It is clearly seen that most of the macroscopic blue regions of liquid nucleation coincide with the bright areas where the field penetrates first. In particular, the correspondence between the arc structures of the penetration field and the melting contours is striking. This correspondence indicates that the melting propagation at low fields is indeed governed by the local variations in T_c. A comparison of the penetration image and the melting contours at $H_a = 75$ Oe reveals surprisingly large anti-correlation behavior. The regions into which the field penetrates first are often the last ones to melt, for example, the 'P–P' strip is bright in figure 2c but is mainly yellow and orange in figure 2b. The anti-correlation behavior causes the observed crossing of the local melting lines as discussed above.

5. Summary

We have studied the vortex melting phenomenon in BSCCO using the sensitive differential magneto-optical imaging technique which enables the observation of local jumps in magnetization of the order of 100 to 300 mG. Contour maps of the nucleation and the evolution of the vortex solid–liquid interface as a function of field or temperature have been constructed. We surmise that competing contributions of different types of quenched random disorder which locally affect T_c or H_0 produce opposite effects on the local melting transition, and we recognize them to be a crucial ingredient in determining the complexity of the melting patterns.

Acknowledgements

This work was supported by the Israel Science Foundation and Center of Excellence Program, by Minerva Foundation, Germany, by the Ministry of Science, Israel, and by the Grant-in-Aid for Scientific Research from the Ministry of Education, Science, Sports and Culture, Japan. EZ acknowledges the support by the Fundacion Antorchas — Weizmann Institute of Science Collaboration Program.

References

[1] Y Imry and M Wortis, *Phys. Rev.* **B19**, 3580 (1980)
[2] G Blatter *et al*, *Rev. Mod. Phys.* **66**, 1125 (1994) and references therein
[3] E Zeldov *et al*, *Nature* **375**, 373 (1995)
[4] E Zeldov *et al*, *Phys. Rev. Lett.* **73**, 1428 (1994)
[5] M V Indenbom *et al*, *Physica* **C166**, 486 (1990)
[6] C A Duran *et al*, *Nature* **357**, 474 (1992)
[7] U Welp *et al*, *Nature* **376**, 44 (1995)
[8] A Soibel *et al*, *Nature* **406**, 282 (2000)
T Tamegai *et al*, *Physica* **C357–360**, 568 (2001)
[9] N Morozov *et al*, *Phys. Rev.* **B54**, R3784 (1996)
[10] B Khaykovich *et al*, *Phys. Rev.* **B56**, R517 (1997)
[11] C M Paulius *et al*, *Phys. Rev.* **B61**, R11910 (2000)
[12] B Khaykovich *et al*, *Phys. Rev.* **B57**, R14088 (1998)
[13] W K Kwok *et al*, *Phys. Rev. Lett.* **84**, 9706 (2000)
[14] B Khaykovich *et al*, *Phys. Rev. Lett.* **76**, 2555 (1996)
[15] A Soibel *et al*, *Phys. Rev. Lett.* **87**, 167001 (2001)
[16] G Blatter and B I Ivlev, *Phys. Rev.* **B50**, 10272 (1994)